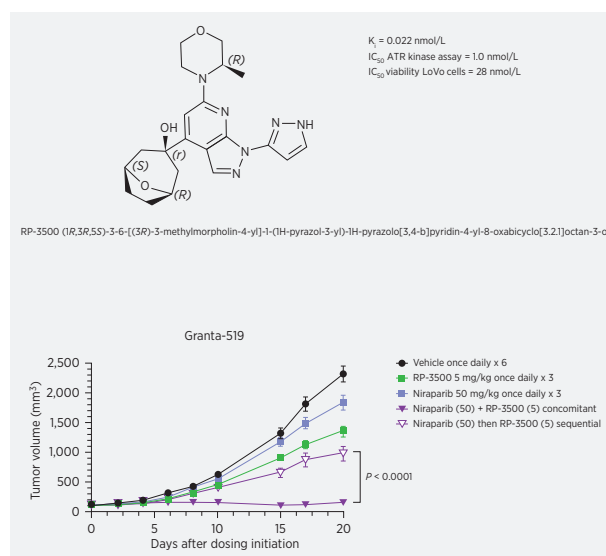# RP-3500: A Novel, Potent, and Selective ATR Inhibitor that is Effective in Preclinical Models as a Monotherapy and in Combination with PARP Inhibitors

Anne Roulston[1], Michal Zimmermann[1], Robert Papp[1], Alexander Skeldon[2], Charles Pellerin[2], Émilie Dumas-Bérube[2], Valerie Dumais[2], Stéphane Dorich[2], Lee D. Fader[2], Sara Fournier[1], Li Li[1], Marie-Eve Leclaire[1], Shou Yun Yin[1], Amandine Chefson[2], Hunain Alam[1], William Yang[1], Chloe Fugère-Desjardins[1], Sabrina Vignini-Hammond[3], Kathryn Skorey[3], Amina Mulani[3], Victoria Rimkunas[1], Artur Veloso[1], Martine Hamel[1], Rino Stocco[1], Yael Mamane[1], Zuomei Li[3], Jordan T.F. Young[1], Michael Zinda[1], and W. Cameron Black[1]

ABSTRACT

Ataxia telangiectasia and Rad3-related (ATR) kinase protects genome integrity during DNA replication. RP-3500 is a novel, orally bioavailable clinical-stage ATR kinase inhibitor (NCT04497116). RP-3500 is highly potent with IC_{50} values of 1.0 and 0.33 nmol/L in biochemical and cell-based assays, respectively. RP-3500 is highly selective for ATR with 30-fold selectivity over mammalian target of rapamycin (mTOR) and more than 2,000-fold selectivity over ataxia telangiectasia mutated (ATM), DNA-dependent protein kinase (DNA-PK), and phosphatidylinositol 3-kinase alpha (PI3Kα) kinases. *In vivo*, RP-3500 treatment results in potent single-agent efficacy and/or tumor regression in multiple xenograft models at minimum effective doses (MED) of 5 to 7 mg/kg once daily. Pharmacodynamic assessments validate target engagement, with dose-proportional tumor inhibition of phosphorylated checkpoint kinase 1 (pCHK1) ($IC_{80} = 18.6$ nmol/L) and induction of phosphorylated H2A.X variant histone (γH2AX), phosphorylated DNA-PK catalytic subunit (pDNA-PKcs), and phosphorylated KRAB-associated protein 1 (pKAP1). RP-3500 exposure at MED indicates that circulating free plasma levels above the *in vivo* tumor IC_{80} for 10 to 12 hours are sufficient for efficacy on a continuous schedule. However, short-duration intermittent (weekly 3 days on/4 days off) dosing schedules as monotherapy or given concomitantly with reduced doses of olaparib or niraparib, maximize tumor growth inhibition while minimizing the impact on red blood cell depletion, emphasizing the reversible nature of erythroid toxicity with RP-3500 and demonstrating superior efficacy compared with sequential treatment. These results provide a strong preclinical rationale to support ongoing clinical investigation of the novel ATR inhibitor, RP-3500, on an intermittent schedule as a monotherapy and in combination with PARP inhibitors as a potential means of maximizing clinical benefit.

K_i = 0.022 nmol/L
IC_{50} ATR kinase assay = 1.0 nmol/L
IC_{50} viability LoVo cells = 28 nmol/L

RP-3500 (1*R*,3*R*,5*S*)-3-6-[(3*R*)-3-methylmorpholin-4-yl]-1-(1H-pyrazol-3-yl)-1H-pyrazolo[3,4-b]pyridin-4-yl-8-oxabicyclo[3.21]octan-3-ol

[1]Repare Therapeutics Inc., Saint-Laurent, Quebec, Canada. [2]Ventus Therapeutics Inc. Saint-Laurent, Quebec, Canada. [3]NuChem Sciences Inc. Saint-Laurent, Quebec, Canada.

Corresponding Author: Anne Roulston, Repare Therapeutics Inc., 7171 Frederick Banting, Saint-Laurent, QC H4S 1Z9, Canada. Phone: 514-286-4789; Fax: 888-595-2535; E-mail: aroulston@reparerx.com

Introduction

Many cancers harbor defects in DNA damage response (DDR) pathways leading to incomplete DNA repair, circumvention of DNA damage checkpoints, and/or the dependence of tumor cells on alternative DNA repair mechanisms. Tumors bearing DNA repair defects therefore possess important vulnerabilities that can be exploited for therapeutic intervention (1).

Ataxia telangiectasia and Rad3-related (ATR) kinase is an important therapeutic target due to its pivotal role in DNA replication and repair. It is a member of the phosphatidylinositol 3′ kinase-related kinase (PIKK) family which also includes the ataxia telangiectasia mutated (ATM) and DNA-dependent protein kinase catalytic subunit (DNA-PKcs) repair kinases. While ATM and DNA-dependent protein kinase (DNA-PK) repair double-strand breaks (DSB) generated from

radiation/chemotherapy or collapsed DNA replication forks, the primary role of ATR is to regulate DNA replication and cell cycle checkpoint activation to ensure complete and intact cell division (2). ATR, with its regulatory partner ATR interacting protein (ATRIP), are recruited to blocked or damaged DNA replication forks. ATR protects stalled replication forks through helicases that remodel their structure to prevent cleavage and then promotes fork repair via homologous recombination (HR) factors such as BRCA2 and partner and localizer of BRCA2 (PALB2) (3). ATR also acts by phosphorylating checkpoint kinase 1 (CHK1) on Ser-345 (pCHK1), causing its activation. Once activated, pCHK1 mediates cell cycle arrest in S or G_2–M phases (2) allowing DNA repair prior to cell cycle progression. Following ATR inhibition, replication stress is increased by compromised fork repair and accumulation of dormant origins of replication. This leads to massive formation of DSBs, activation of ATM and DNA-PKcs followed by phosphorylation of their substrates KRAB-associated protein 1 (KAP1) and H2AX, and irreversible collapse of DNA replication known as replication catastrophe (3–5). ATR inhibition also impairs cell cycle checkpoint control, which prematurely forces cells into mitosis in the presence of DNA damage and an incompletely replicated genome, resulting in chromosome fragmentation and mitotic cell death (6).

Several orally available ATR inhibitors (ATRi) including AZD6738 (7, 8), M4344 (9), BAY1895344 (10, 11), M1774 (12), ATR0380 (NCT04657068), and ATRN-119 (NCT04905914) are currently undergoing clinical evaluation and have tolerability profiles as single agents with toxicities including myelosuppression, fatigue, and gastrointestinal effects (13). Clinical single-agent ATRi efficacy has been reported for BAY1895344 and AZD6738 in a small number of patients with selected DDR deficiencies including *BRCA1/2* mutations, ATM loss of function, or tumors with unreported genomic alterations, suggesting an early proof of concept for this drug class (8, 14, 15).

Given the role of ATR during DNA replication, it is not surprising that upon ATR inhibition cells rely on genes such as *ATM* and *BRCA1/2* to mediate DSB repair caused by collapsed replication forks and loss of HR (16–21). In addition, several recent studies have demonstrated synergy between ATRi and PARP inhibitors (PARPi) in ATM and BRCA1/2-deficient preclinical models (22–26).

Synergy between ATRi and PARPi has been widely reported and is a promising clinical strategy; however, continuous combination treatment has been poorly tolerated preclinically (22–24) and clinically due to myelosuppression (13, 27). Inhibition of PARP activity not only impairs single-strand DNA break repair but also stabilizes PARP-DNA complexes (PARP trapping), leading to replication fork stalling and collapse (28). Both effects cause the accumulation of DSBs during DNA replication and a dependency on HR for repair. Furthermore, *BRCA1* and *BRCA2* mutant cells that have become resistant to PARP inhibition by bypassing the replication fork protection roles of these HR proteins, are also dependent on ATR for essential DNA repair functions (22, 25).

ATR inhibition in the presence of PARPi results in premature entry into mitosis, leading to mitotic catastrophe and cell death (26, 29, 30). In preclinical cancer models, ATRi and PARPi combinations demonstrated synergistic enhancement of cell death and tumor regression (10, 22, 25, 26); however, tolerability was limited by both the dose level and duration of administration. Clinically, combining an ATRi and PARPi leads to overlapping toxicities, including myelosuppression, limiting tolerability (30). Additional work is needed to establish dose scheduling to optimize these combinations for clinical use.

This is the first disclosure of the structure of RP-3500, a novel, oral ATRi currently under clinical evaluation (NCT04497116). RP-3500 is highly selective and inhibits ATR at picomolar to nanomolar concentrations in biochemical and cell-based assays. RP-3500 is highly efficacious as a monotherapy in several preclinical models that are BRCA1-deficient or that have deficits of ATM pathway function. Here, we demonstrate that the therapeutic index of RP-3500 is widened when administered on an intermittent dosing schedule to mitigate on-target hematologic toxicity associated with continuous dosing. Furthermore, the benefits of intermittent dosing extend to PARPi combinations where attenuated doses of RP-3500 with either niraparib or olaparib administered concomitantly were substantially more efficacious and better tolerated than sequential administration of the combination.

Materials and Methods

Test compounds

RP-3500 (1*R*,3*R*,5*S*)-3–6–[(3*R*)-3-methylmorpholin-4-yl]-1-(1H-pyrazol-3-yl)-1H-pyrazolo[3,4-b]pyridin-4-yl-8-oxabicyclo[3.2.1]octan-3-ol was prepared as described for Example 121 of WO2020/087170 (Supplementary Methods; ref. 31). Gemcitabine, bleomycin (Sigma, #G6423, #B5507), niraparib, and olaparib (MedChem Express, #HY-10619, #HY-10162) were purchased.

Cell lines

Capan-1, CW-2, NCI-H23, LoVo, MDA-MB-436, SNU-601, and HT-29 cells were obtained from ATCC, Granta-519 cells from DSMZ, and SUM149PT from Asterand in 2018, and were not further authenticated. RPE1-hTERT *TP53KO ATM*—wild-type (*WT*) and *ATM*-knockout (*KO*) cells were made as described in the Supplementary Methods. Cells were cultured as recommended and were verified *Mycoplasma* and murine pathogen free, quarterly by PCR (internally and at Idexx Bioanalytics). Cells were cultured up to 10 weeks and were used at passages of less than 20 from the initial source vial.

Cell viability

Cells were plated 24 hours before treatment at optimal densities for each line (200–2,500 cells per well) in 96-well plates (Corning, #3903), then treated with compound for 120 hours before determining cell viability using CellTiter-Glo (Promega, # G7571). Luminescence was read on either Envision 2105 (Perkin-Elmer), SpectraMax M3, or FlexStation 3 (Molecular Devices) plate readers. Cell viability was calculated by normalizing each blank-corrected luminescence value to untreated cells. Synergy between RP-3500 and PARPi was determined with SynergyFinder (https://synergyfinder.fimm.fi) using the Zero interaction potency (ZIP) model (32).

Immunoblotting

Cells and tumor fragments were lysed in a buffer (Mesoscale discovery, #R60TX-2) with protease and phosphatase inhibitors (Thermo Fisher Scientific, #78437; Thermo Fisher Scientific, #78420). Lysates were separated by SDS-PAGE (Bio-Rad, #5678085); then transferred to polyvinylidene fluoride membranes. Membranes were incubated with primary antibodies: anti-pCHK1 (Ser345; Cell Signaling Technology, #2348), anti-pKAP1(S824; Abcam; catalog no. ab133440), anti-KAP1 (Abcam; catalog no. 10484), anti-ATM (Novus; NB100–104SS) and anti-pDNA-PKcs (Abcam; catalog no. 124918), anti-CHK1 (Cell Signaling Technology, #2348), or anti-γH2AX (EMD Millipore; catalog no. 05–636). Signal detection was carried out with secondary anti-rabbit (Jackson Immuno Research, #711–035–152) or anti-mouse (Jackson Immuno Research, #115–035–174) horseradish peroxidase (HRP) antibody and Super-Signal West Dura Extended Duration Substrate (Thermo Fisher

Scientific, #34076) using a Bio-Rad ChemiDoc Touch Imaging System (Bio-Rad, #1708370).

Biochemical kinase assays

ATR biochemical assays used human recombinant tagged proteins ATR/ATRIP (Eurofins, Item#14–953) purified from mammalian cells. Assays were conducted using glutathione S-transferase–tagged p53 substrate (Enzo Lifesciences; catalog no. BML-FW9370–0050) and 3 μmol/L ATP in 50 mmol/L HEPES, 0.01% Brij, 0.1 mmol/L EGTA, and 1% glycerol. Phosphorylated substrate was incubated with anti-phospho-p53 (Ser15) antibody (NEB; catalog no. 9284), donor (Perkin Elmer, 6765301), and acceptor (Perkin Elmer, 670137M) beads for 4 to 5 hours in 60 mmol/L EDTA, 50 mmol/L Tris pH 7.4 with 1.0 mg/mL BSA. Phosphorylation was quantified by fluorescence measured in a BMG Polarstar plate reader (excitation 680 nm, emission 520–620 nm). Standard PIKK and related kinase assays (Kinase Profiler) were performed at Eurofins Discovery, using standard assay protocols. See Supplementary Methods.

ATR, mTOR, and PI3Kα cellular assays

ATR, mTOR, and PI3Kα assays were conducted in LoVo cells as described in the Supplementary Methods, using AlphaScreen and AlphaLISA SureFire assay kits carried out according to the manufacturers' instructions.

ATM and DNA-PK cellular assays

HT-29 cells were plated in 24-well plates (VWR, #10062–896) at 350,000 cells/well. The following day, RP-3500 was added for 60 minutes followed by 3 mU/mL bleomycin (Sigma, #B5507) for 2 hours. Cells were washed with PBS and lysed in MSD Lysis Buffer (Mesoscale discovery, #R60TX-2) supplemented with phosphatase and protease inhibitors (Thermo Fisher Scientific, #78437 and #78420). Phosphorylated ATM substrate pKAP1 (Ser824) was detected by immunoblotting, and DNA-PK activation measured with pDNAPKcs-S2056 (Abcam, #124918) and an HRP-coupled secondary antibody (Jackson Immuno Research, #711–035–152). Membranes, first probed to detect pKAP1 or pDNA-PK, were then stripped with Restore Plus Western Blot Stripping Buffer (Thermo Fisher Scientific, #46430) and reprobed as described above to detect total KAP1 (Abcam, #ab10484) or total DNA-PKcs (Sigma, #MABC1236).

γH2AX immunofluorescence and high-content microscopy

Treated RPE1-hTERT Cas9 *TP53-KO ATM WT* or *ATM-KO* cells at the experimental endpoint, were rinsed in PBS, fixed with 4% para-formaldehyde/PBS, and permeabilized in 0.3% Triton X-100/PBS. Cells were subsequently blocked in polybenzyl glutamate (0.2% cold water fish gelatin, 0.5% BSA in PBS) and incubated with a primary mouse anti–γH2AX antibody clone JBW301 (Millipore Sigma, 05–636). Cells were rinsed and incubated with an Alexa Fluor 488-conjugated goat anti-mouse IgG secondary antibody (Invitrogen) and 0.5 mg/mL 4′,6-diamidino-2-phenylindole, and then rinsed and imaged on an Operetta automated high-content confocal microscope (Perkin Elmer). Image analysis was performed using Harmony software (Perkin Elmer). Built-in algorithms were used to quantify the mean nuclear γH2AX intensity.

In vivo xenograft studies

All cells were implanted subcutaneously (at 5×10^6 cells/mouse) into the flanks of female mice (6–8 weeks old; Charles River) in a suspension of 1:1 media:Matrigel (Matrigel Corning; catalog no. CB35248). Lovo cells were implanted into CB17 severe combined immunodeficiency (SCID) mice at Repare Therapeutics. CW-2 cells were implanted at NuChem Sciences Inc. and SUM149PT cells at Oncodesign into NOD/SCID. The above studies were conducted in Canadian Council on Animal Care–accredited vivariums with Institutional Animal Care Committee–approved protocols.

Granta-519 cells (1×10^7 cells/mouse) were implanted into female NOD/SCID mice in 1:1 matrigel:PBS at Crown Biosciences Inc. Patient-derived xenograft (PDX) tumor fragments were cut into small pieces (approximately 2–3 mm in diameter) and implanted subcutaneously into female BALB/c nude mice and subsequently passaged by implantation into the efficacy cohort at Crown Biosciences Inc. The procedures involving the care and use of animals for Granta-519 and PDX studies were reviewed and approved by the Institutional Animal Care and Use Committee of Crown Biosciences Inc. prior to execution. During the study, the care and use of animals was conducted in accordance with the regulations of the Association for Assessment and Accreditation of Laboratory Animal Care (AAALAC).

Animals were monitored for tumor volume, clinical signs, and body weight three times per week. Tumor volume was measured using a digital caliper and calculated using the formula $0.52 \times L \times W^2$. Mice were randomized to treatment groups when tumors reached 100 to 200 mm^3. RP-3500, olaparib, and niraparib were administered in 0.5% methylcellulose/0.02% SDS vehicle. See Supplementary Methods for data analysis and statistics.

Pharmacokinetics and pharmacodynamic markers

Mouse whole blood was collected at 0.5, 1, 3, 8, and 24 hours postdose by tail snip and diluted 1:3 with 0.1 mol/L citrate buffer. Plasma was collected from whole blood drawn by cardiac puncture at 1 and 3 hours postdose into tripotassium (K_3) EDTA tubes (Sarstedt; catalog no. 41.1504.105), then centrifuged at 12,000 relative centrifugal force for 10 minutes at 4°C. The concentration of RP-3500 in whole blood and plasma was determined by high-performance LC/MS (see Supplementary Methods). Excised tumors were flash-frozen for protein extract or preserved in 10% formalin. Frozen fragments were homogenized in lysis buffer (Mesoscale discovery, #R60TX-2) with protease and phosphatase inhibitors (Thermo Fisher Scientific, #78437; Thermo Fisher Scientific, #78420) using 2.8-mm ceramic bead-containing tubes (OMNI, #19–628) and a Bead Ruptor 24 (OMNI International). The levels of pCHK1(Ser345), total CHK1, pKAP1(Ser824), total KAP1, and pDNA-PKcs (Ser2056) were determined by immunoblotting relative to untreated controls as described above. The LoVo tumor IC$_{80}$ for pCHK1(Ser345) was determined by a nonlinear least-squares regression to a normalized dose-response four-parameter fit model (GraphPad Prism v9).

Hematology

At the designated endpoint, whole blood was collected from anesthetized mice into K_3-EDTA BD Microtainer MAP Microtubes (Thermo Fisher Scientific, 22–253–270) by cardiac puncture. Hematology analysis was performed with a Sysmex XN-1000™ hematology Analyzer (Sysmex America Inc.).

Results

RP-3500 is a highly potent and selective inhibitor of ATR kinase

To determine the potency of RP-3500 (**Fig. 1A**), a biochemical assay for ATR/ATRIP inhibition was established using tagged human ATR and ATRIP purified from mammalian cells, with p53 (Ser15) as the phosphorylation substrate. In this assay, the Km for ATP was 30 nmol/L and biochemical assays were conducted at 3 μmol/L ATP
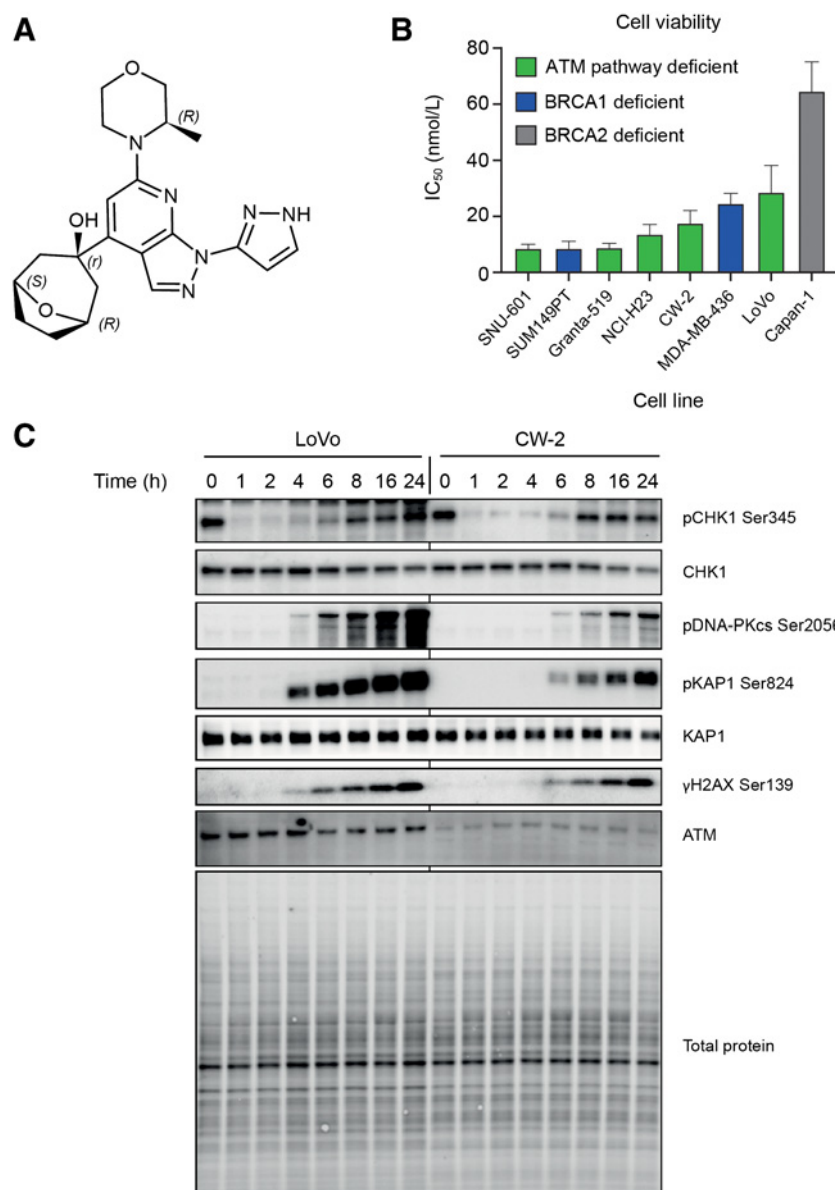
Figure 1.
RP-3500 is a potent ATR kinase inhibitor. **A,** Chemical structure of RP-3500. **B,** Cell growth inhibition in a panel of cell lines with defective ATM or BRCA1/2 pathways measured in a 5-day CellTiter-Glo assay. IC_{50} values were calculated using a dose-response curve normalized to DMSO-treated cells (Prism v7.02). Mean ± SD; $n \geq 3$ independent experiments. **C,** ATR kinase targets or DNA damage markers detected by immunoblotting lysates from ATM pathway-defective human cancer cell lines treated with 1 µmol/L RP-3500 for the indicated times. h, hours.

Table 1. The potency and selectivity of RP-3500 in biochemical and cell-based assays.

Assay IC_{50} (nmol/L)	ATR	mTOR	ATM	DNA-PK	PI3Kα
Biochemical	1.0	120	>30,000	1,600	>10
Selectivity	–	120x	>30,000x	1,600x	>10,000x
Cell-based	0.33[a]	11[b]	>10,000[c]	>10,000[c]	780[b]
Selectivity	–	30x	>20,000x	>20,000x	2,200x

[a]ATR activity induced with gemcitabine in LoVo cells using pCHK1 (Ser345) as a substrate.
[b]mTOR and PI3Kα endogenous kinase activity in unstimulated LoVo cells using pP70S6K (Thr389) and pAKT1 (Thr308) as substrates, respectively.
[c]ATM and DNA-PK activity induced with bleomycin in HT-29 cells using pKAP1 (Ser824) and pDNA-PKcs (Ser2056) as substrates, respectively.

where the IC_{50} of RP-3500 was 1.00 ± 0.40 nmol/L (**Table 1**) and the Ki was 0.022 ± 0.002 nmol/L. In a LoVo cell-based assay, the IC_{50} of RP-3500 to inhibit gemcitabine-stimulated ATR phosphorylation of its substrate pCHK1(Ser345) was 0.33 nmol/L (**Table 1**). The potency in biochemical assays is consistent with low nanomolar growth inhibitory activity ($IC_{50} = 8–64$ nmol/L) in cell viability assays in a panel of cell lines with defective ATM or BRCA1/2 function (**Fig. 1B**; Supplementary Table S1). These results demonstrate that RP-3500 is a potent ATRi in both biochemical and cell-based assays.

To determine selectivity within the kinome, RP-3500 was incubated with a Jurkat whole-cell lysate, and the ability of an ATP-binding pocket probe to displace RP-3500 was determined by mass spectrometry (Supplementary Fig. S1A and S1B; ref. 33). RP-3500 demonstrated high selectivity for ATR. At 3 nmol/L, RP-3500 remained bound to 82.8% of ATR in the lysate but not to any of the other evaluable kinases.

At 300 nmol/L, RP-3500 showed no binding activity to more than 300 kinases outside of the PIKK family. Weak binding was detected to five PIKK or PI3K family members. To confirm RP-3500 selectivity, specific cell-based kinase assays were developed to determine the intracellular inhibitory activity within the PIKK family. In each assay, RP-3500 showed weak inhibition of PIKK family cellular kinase activity resulting in 30-fold selectivity over mTOR and more than 2,000-fold selectivity over ATM, DNA-PK, and PI3Kα kinases (**Table 1**).

To characterize the DDR to RP-3500–mediated ATR inhibition, LoVo and CW-2 human colon cancer cell lines were treated with 1 μmol/L of RP-3500 for various durations up to 24 hours, the dose being chosen to inhibit more than 90% of endogenous CHK1 phosphorylation. RP-3500 inhibits CHK1(Ser345) phosphorylation from 1 to 3 hours after treatment initiation. However, starting at 4 hours, CHK1(Ser345) became rephosphorylated as DNA-PKcs became activated in treated cells, along with its substrates KAP1 and H2AX (**Fig. 1C**), demonstrating induction of DSB DNA damage (34).

RP-3500 is active as a single agent in xenograft models

RP-3500 showed single agent activity in several xenograft models of gastric and colon cancer with dysfunctional ATM pathways. LoVo cells express WT *ATM* but have an *MRE11A* splicing deficiency (functionally ATM-compromised; ref. 35), while CW-2 cells have an *ATM* missense mutation (A2843V; ref. 36) resulting in low ATM expression (**Fig. 1C**). Administration of RP-3500 once daily to mice bearing LoVo xenografts produced dose-dependent tumor growth inhibition with an MED of 7 mg/kg (**Fig. 2A**). Similarly, administration of RP-3500 at a dose of 5 and 10 mg/kg once daily produced statistically significant tumor growth inhibition in the CW-2 colon xenograft model (Supplementary Fig. S2A). Despite tumor-induced cachexia in both models, RP-3500 doses of 3 to 10 mg/kg daily were well tolerated with minimal additional body weight loss relative to vehicle control (Supplementary Fig. S2B and S2C). At 15 mg/kg, 1 mouse was sacrificed due to body weight loss (after day 12) and the remaining mice experienced more than 15% body weight loss. Therefore, the MTD was 10 mg/kg once daily on a continuous dosing schedule. In a PDX model of gastric cancer with ATM protein loss (Supplementary Fig. S2D), RP-3500 was highly efficacious, eliciting complete tumor regressions at 5 and 10 mg/kg daily (**Fig. 2B**) without body weight loss at either dose level (Supplementary Fig. S2E). These results demonstrate a low single-agent MED of RP-3500 (5–7 mg/kg daily) in multiple tumor models (Supplementary Table S2), with potential for complete regression.

To verify target engagement *in vivo* and establish a pharmacokinetic (PK)/pharmacodynamic (PD) marker relationship, plasma and tumors were sampled from the LoVo tumor model at 1 and 3 hours posttreatment and analyzed for circulating levels of RP-3500 and tumor pCHK1 by immunoblotting. A clear proportional relationship between pCHK1 inhibition and circulating free plasma levels of RP-3500 was demonstrated with an estimated tumor target engagement IC_{80} of 18.6 nmol/L [85% confidence interval (CI), 7.23–145 nmol/L] (**Fig. 2C**).

To determine the exposure levels needed to achieve minimum efficacy, the PK profile of RP-3500 was measured at steady state at several doses (**Fig. 2D**). The circulating free plasma levels of RP-3500 at the MED range of 5 to 7 mg/kg support the idea that an RP-3500 free concentration above the *in vivo* tumor IC_{80} for 10 to 12 hours is sufficient for efficacy. This is considered a conservative estimate based on the modest RP-3500 sensitivity of the LoVo xenograft relative to other cell line tumor models (**Fig. 1B**).

DNA DSBs induced by ATR inhibition cause DNA damage marked by phosphorylated H2AX (γH2AX) and KAP1 (pKAP1; ref. 2), and are proposed as useful clinical pharmacodynamic biomarkers for ATRi (12, 14, 37). Mice bearing LoVo tumors were treated for 7 days, and tumor tissue harvested 24 hours after the last RP-3500 treatment, consistent with the timing of the DDR seen in **Fig. 1C**. Dose-dependent KAP1 and DNA-PKcs phosphorylation was detected by immunoblotting resulting in 8.1- and 2.7-fold inductions, respectively, over background levels at 7 mg/kg RP-3500 (**Fig. 2E**; Supplementary Fig. S2F). Similarly, gastric PDX tumor tissues with biallelic ATM loss sampled 24 hours after three daily treatments showed dose-proportional IHC staining of γH2AX and pKAP1 (**Fig. 2F**). Quantitation of the signal in tumor tissue indicated a 2.8- and 4.4-fold induction for γH2AX and a 6.7- and 18.4-fold induction for pKAP1 over background with 5 and 10 mg/kg RP-3500, respectively, confirming the induction of DNA damage and reinforcing the proposed use of these molecular markers of tumor response in early clinical trials.

A weekly intermittent administration schedule mitigates toxicities associated with in *in vivo* ATR inhibition

To optimize an *in vivo* RP-3500 administration schedule, washout experiments were conducted *in vitro* to determine the exposure required to generate irreversible DNA damage. These experiments were performed in an engineered isogenic cell line pair (RPE1-hTERT Cas9 *TP53-KO ATM-WT* and *ATM-KO*) where the sensitivity of the *ATM-KO* cell line was six-fold greater than the *ATM-WT* line (Supplementary Fig. S3A and S3B). Exposure to 30 nmol/L RP-3500 for 48 and 72 hours increased γH2AX staining to similar levels in both the *ATM-WT* and *ATM-KO* cells. However, when compound was removed after a 72-hour exposure, the *ATM-WT* cells mostly recovered from γH2AX–marked DNA damage after 24 hours, whereas the cells lacking functional ATM had sustained DNA damage for at least 48 hours (**Fig. 3A** and **B**). Consistent with these results, treatment of Granta-519 cells (*ATM* LOF mutation) with RP-3500 for longer than 2 to 3 days did not result in significant lowering of the IC_{50}. Together, these results suggest that short-term exposure to RP-3500 is sufficient to cause irreparable DNA damage and induce growth inhibition (Supplementary Fig. S3C and S3D).

To examine the effects of intermittent RP-3500 administration on tolerability and efficacy, the MTD was determined for weekly treatment schedules of 2 days on/5 days off, 3 days on/4 days off, and 5 days on/2 days off. The daily MTDs for the three schedules were 30, 30, and 25 mg/kg, respectively, demonstrating that increased dose levels of RP-3500 are tolerated with intermittent schedules compared with continuous daily administration (MTD of 10 mg/kg; Supplementary Fig. S3E). Firstly, three daily doses weekly is sufficient to maximize antitumor efficacy of the 10 mg/kg dose, consistent with *in vitro* results (Supplementary Fig. S3F and S3G). Secondly, a more profound antitumor effect occurred at higher doses on the 3 days on/4 days off and 5 days on/2 days off schedules compared with consecutive daily administrations at a lower dose (**Fig. 3C**; Supplementary Table S2). This suggests that a dose of RP-3500 (30 mg/kg) providing IC_{80} target inhibition for 24 hours/day for 3 days is more efficacious than a dose (10 mg/kg) providing target inhibition approximately 16 hours/day for 7 days (**Fig. 3C**; Supplementary Fig. S3H).

Anemia is a known adverse effect of ATRi, observed in both the preclinical and clinical settings (8, 14, 38). Therefore, hematologic toxicity was evaluated in mice after 2 weeks of RP-3500 treatment as a more sensitive measure of tolerability than body weight loss. Although body weight loss was somewhat increased for the longer-duration
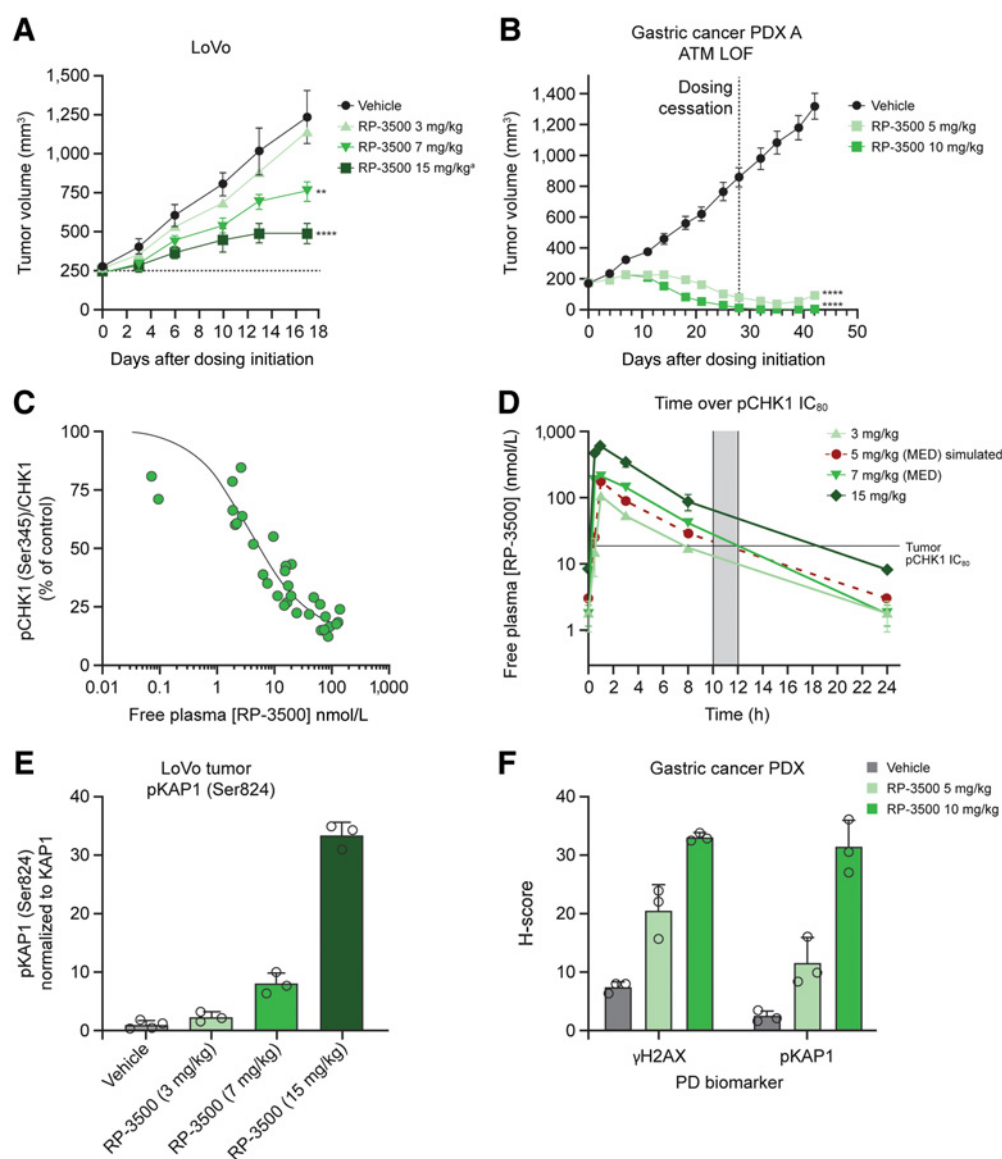
Figure 2.
RP-3500 is efficacious as a single agent in ATM-deficient tumor models. **A,** LoVo tumor xenograft volume in mice treated with RP-3500 orally once daily × 17 days. Results are expressed as mean ± SEM, $N = 10$/group. [a]One mouse sacrificed due to body weight loss on day 12. **B,** Tumor volume of a human gastric cancer PDX A with a biallelic loss of *ATM* in mice treated with RP-3500 at 5 and 10 mg/kg once daily x 28 days. Results expressed as mean ± SEM, $N = 10$/group. Statistical significance relative to vehicle control for **A** and **B** established by one-way ANOVA with Fisher LSD test; $**P < 0.01$; $****P < 0.0001$. **C,** Proportion of pCHK1 (Ser345) inhibition relative to circulating free RP-3500 plasma levels. Tumors and plasma sampled at 1 and 3 hours after RP-3500 administration. The pCHK1/total CHK1 signal is represented relative to vehicle-treated tumors. **D,** Free circulating plasma concentrations of RP-3500 over time in SCID mice. Green, measured concentrations; red, simulated PK at 5 mg/kg. Horizontal line indicates *in vivo* LoVo tumor pCHK1 IC$_{80}$ determined by nonlinear curve fit of **C**. Vertical grey bar indicates window of duration over IC$_{80}$ at the MED (5–7 mg/kg). h, hours. **E,** pKAP1 (Ser824) in LoVo tumors from mice treated with RP-3500 once daily x 7 days and harvested 24 hours after the last dose. pKAP1/total KAP1 quantified by immunoblot are represented as fold increase over vehicle control signal. **F,** Quantitative γH2AX and pKAP1 staining of tissue sections from the gastric PDX-bearing mice treated with RP-3500 once daily for 3 days harvested 24 hours after the last dose. PD, pharmacodynamics.

weekly dosing schedules (Supplementary Fig. S3E), these schedules (5 and 7 days on per week) also resulted in increasingly dramatic reductions in red blood cell (RBC) count (**Fig. 3D**). Intermittent dosing schedules with a dose holiday of at least 4 consecutive days was sufficient to allow reticulocyte regeneration above the vehicle control values (**Fig. 3E**), demonstrating that erythroid toxicity resulting from sustained target inhibition over 3 days is reversible given a sufficient recovery time. These results imply that intermittent dose holidays

increase the therapeutic index and support the clinical evaluation of intermittent administration schedules in monotherapy settings.

Short concomitant treatment with RP-3500 and the PARPi olaparib synergizes more than sequential treatment

To investigate whether intermittent schedules of RP-3500 and PARPi combination therapy could provide the same tolerability and efficacy benefits of single-agent intermittent dosing, synergy was first
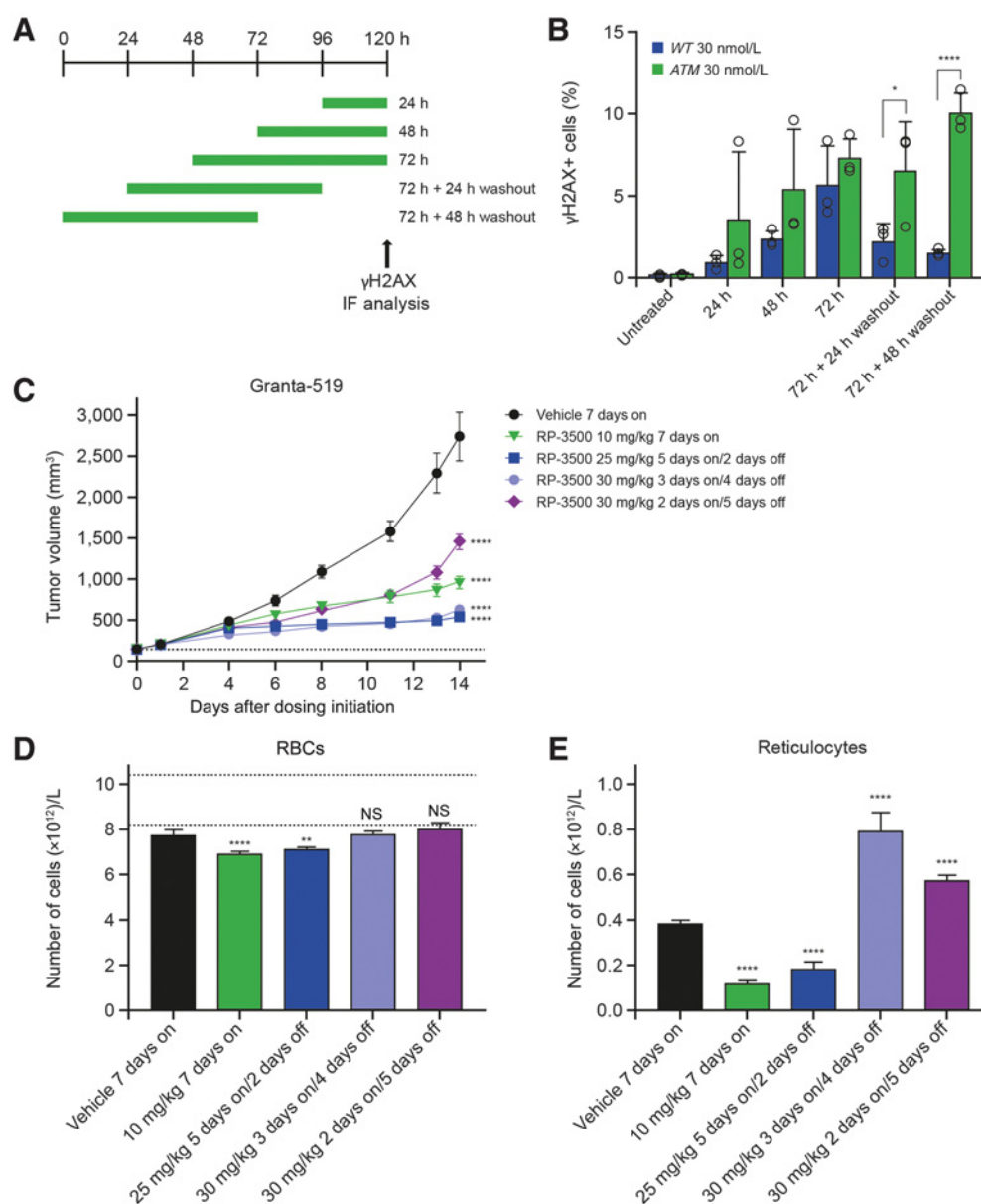
Figure 3.
Intermittent dose scheduling for RP-3500 improves efficacy while minimizing toxicity. **A** and **B,** *In vitro* treatment of RPE1-hTERT Cas9 *TP53-KO ATM WT* and *ATM KO* cells with RP-3500 (30 nmol/L; in green) followed by washout periods and stained with nuclear γH2AX by immunofluorescence (IF) after 120 hours. Mean ± SD; *N* = 3 independent experiments. **C,** Tumor xenograft volume. **D,** Red blood cell; and **E,** Reticulocyte counts from mice bearing Granta-519 tumors treated orally with RP-3500 at MTD on different weekly dosing schedules. RP-3500 was administered once daily according to the indicated schedule. Blood parameters were measured on day 14. Mean ± SEM, *N* = 9/group. Dashed lines indicate reference RBC range from female, age- and strain-matched mice (Charles River). Statistical significance relative to vehicle control was established by one-way ANOVA with Fisher LSD test (GraphPad Prism v9). *$P < 0.05$; **$P < 0.01$; ****$P < 0.0001$, NS, not significant; h, hours.

examined *in vitro*. The SUM149PT *BRCA1*-mutated breast carcinoma cell line (39) was exposed to a 3-day concomitant or 3-day sequential combination of RP-3500 and olaparib with endpoint viability measured at day 8 (**Fig. 4A**). The overall combined effects of RP-3500 and olaparib were more synergistic (maximum ZIP synergy score >10) when administered concomitantly compared with sequential olaparib treatment first (**Fig. 4B**). Importantly, synergy between RP-3500 and olaparib occurred at lower concentrations of each agent (**Fig. 4C**) and a

greater tumor cell-killing effect was observed (**Fig. 4D**) with concomitant treatment compared with sequential treatment.

In vivo, low dose PARPi with concomitant RP-3500 produces greater antitumor effects compared with sequential administration without affecting tolerability

Given the synergy observed between RP-3500 and a PARPi in cell-based assays, concomitant and sequential administration schedules
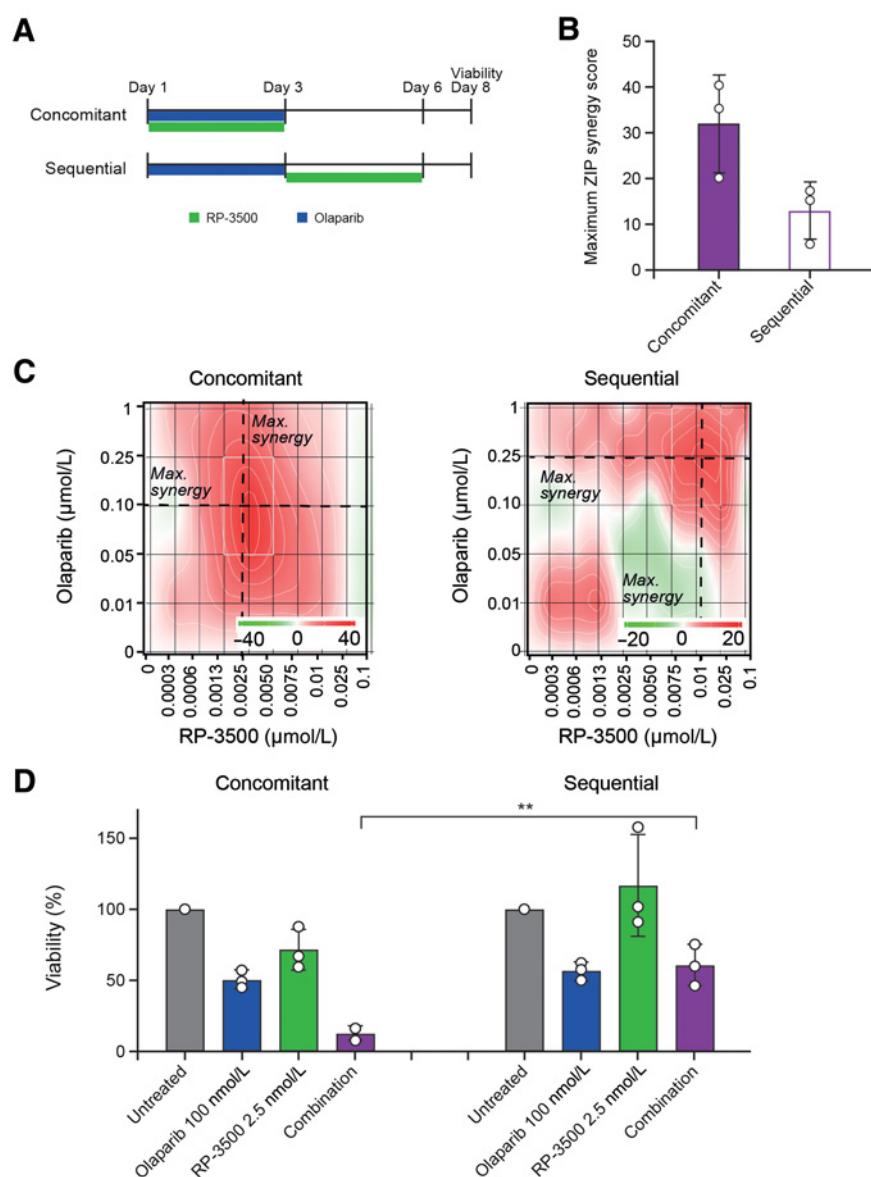
Figure 4.
Concomitant treatment with RP-3500 and olaparib is more synergistic and effective than sequential treatment in *BRCA1* mutated SUM149PT cells. **A,** *In vitro* RP-3500 and olaparib combination treatment schedule in SUM149PT cells with endpoint viability measured at day 8 by CellTiter-Glo. **B,** Maximum ZIP synergy scores for each schedule (SynergyFinder; ref. 32). **C,** The synergy matrix ZIP score for concomitant and sequential compound treatment. Score ≥10, (red) synergy; ≤−10 (green) antagonism; dashed lines, concentrations of each agent generating maximum synergy. Max., maximum. **D,** Viability of cells treated with either RP-3500, olaparib, or the combination at the indicated concentrations and schedules as in **A**. Values represent the percent viability relative to untreated controls. Circles are values from three independent biological replicates; bars indicate mean ± SD. *P* values calculated with a two-tailed unpaired Student *t* test; **P* < 0.01.

were also compared in xenograft models with olaparib and niraparib to evaluate efficacy and tolerability. Mice were treated on weekly concomitant (both agents days 1–3 on/4 days off) or sequential (PARPi for 3 days followed by RP-3500 for 3 days, then 1 day off) schedules (**Fig. 5A**). Mice bearing SUM149PT tumors were treated for 5 weeks with either a concomitant or sequential intermittent RP-3500 + olaparib combination at dose levels below the MTD of each agent alone. All combinations were well tolerated with no significant body weight loss (Supplementary Fig. S4A) or PK drug–drug interactions (Supplementary Fig. S5A and S5B) for the treatment duration. As observed *in vitro*, the efficacy of the RP-3500/olaparib combination was significantly better when administered concomitantly compared with sequentially and was better than RP-3500 alone at its MTD (**Fig. 5B**; Supplementary Table S3). Importantly, intermittent concomitant administration was tolerated over 5 weeks of treatment and resulted in sustained antitumor activity for 3 weeks after dosing cessation in contrast to sequential administration where tumor growth continued over the course of the experiment.

Similarly, in mice bearing Granta-519 tumors, concomitant administration of RP-3500 and niraparib was more effective than sequential administration over a 3-week period, with no terminal body weight loss or difference in RBC count (**Fig. 5C** and **D**; Supplementary Fig. S4B). In this model, the combination was more efficacious and better tolerated (body weight and anemia) than high-dose niraparib as a single agent (70 mg/kg 5 days weekly) and did not cause meaningful drug–drug interactions (Supplementary Fig. S5B). A surge in the appearance of reticulocytes was observed with the 3 days on/4 days off concomitant schedule after 4 days off drug, suggesting that the intermittent RP-3500 and PARPi schedule permits regeneration of the RBC compartment, in contrast to sequential administration that causes more profound anemia and lower reticulocyte count relative to vehicle (**Fig. 5E**). For comparison, the same low dose levels of RP-3500 and niraparib were administered continuously for 7 days weekly in combination and were not tolerated, with 2 of 6 mice sacrificed on day 19 due to body weight loss and remaining mice showing severe anemia and ablation of reticulocytes on day 21 (Supplementary

Figure 5.
Low-dose PARPi administered concomitantly on an intermittent schedule with RP-3500 is more effective without additional toxicity *in vivo*. **A,** Combinations of RP-3500 with olaparib or niraparib were administered on the schedule shown with concomitant or sequential (PARPi first) weekly schedule. Tumor xenograft volume from SUM149PT (**B**) or Granta-519 (**C**) tumor-bearing mice. Mean ± SEM; $N = 9$ mice/group. Mice were treated orally with RP-3500 once daily for 3 days and **B,** Olaparib twice daily for 3 days; or **C,** Niraparib once daily for 3 days or 5 days at the doses indicated. **D** and **E,** Blood parameters measured on day 21 from Granta-519 tumor-bearing mice; mean ± SEM; $N = 9$ mice/group. Dashed lines indicate reference RBC range from female age- and strain-matched mice (Charles River). Statistical significance relative to vehicle control was established by one-way ANOVA with Fisher LSD test (GraphPad Prism v9). NS, not significant. $*P < 0.05$, $**P < 0.01$, $***P < 0.001$, $****P < 0.0001$.
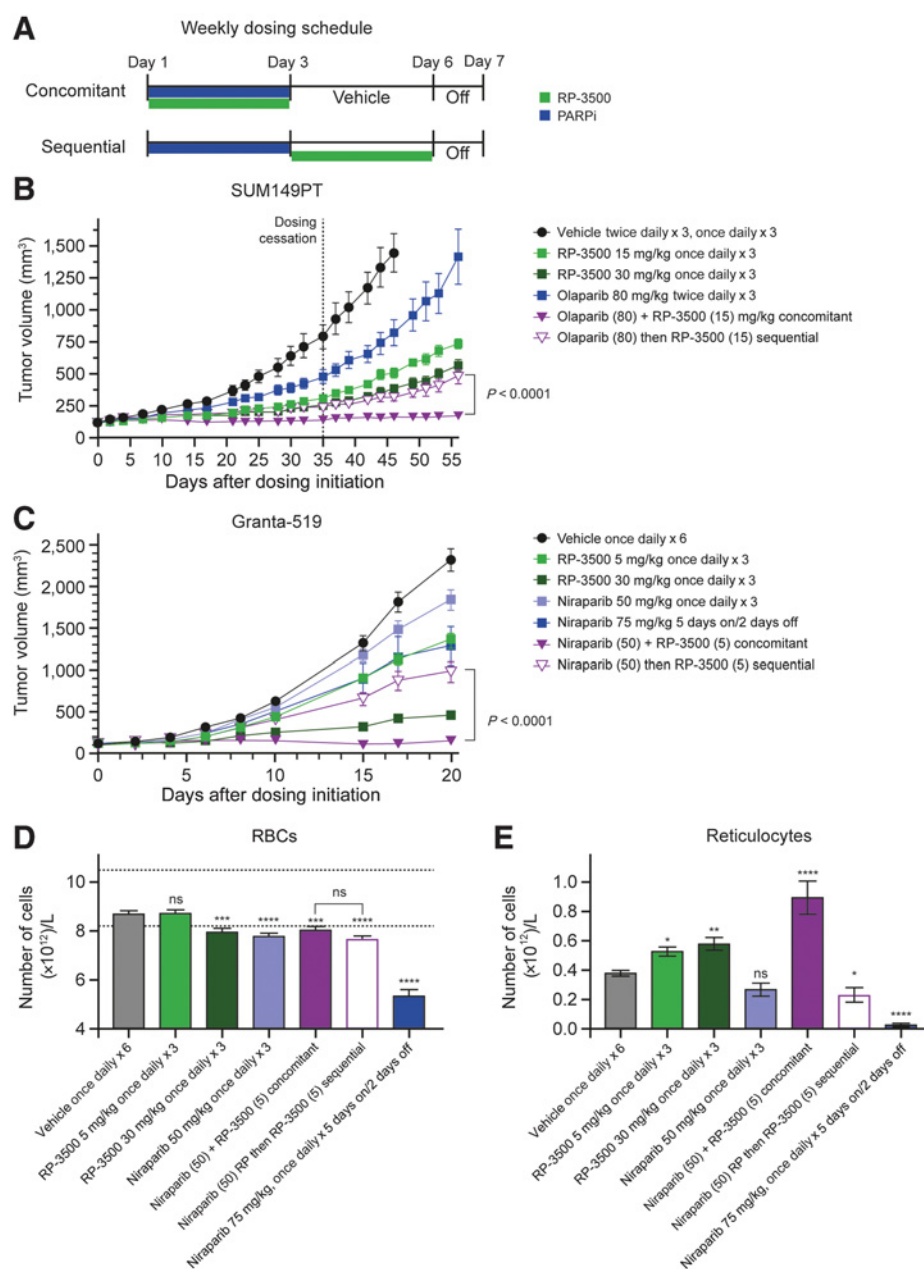
Fig. S4C–S4E). Together, these results demonstrate that an intermittent concomitant rather than sequential administration of RP-3500 + PARPi generates stronger antitumor responses without increased anemia.

Discussion

In this first disclosure, we show that RP-3500 is a highly potent and selective ATRi in biochemical and cell-based assays with a preclinical pharmacology profile that justifies clinical evaluation. In cell assays, RP-3500 inhibits ATR with an IC_{50} of 0.33 nmol/L, and is 30-fold selective over mTOR and more than 2,000-fold selective over other PIKK family members including ATM, DNA-PK, and the related kinase PI3Kα, showing that RP-3500 is among the most potent (9) and selective published ATRi (5, 10, 40–42). RP-3500 is orally bioavailable *in vivo* with compelling efficacy when administered daily as a single agent in the LoVo model with an MED of 7 mg/kg once daily compared with the published MED for AZD6738 of 25 mg/kg once daily in the same model (5). Similarly, in the Granta-519 model, RP-3500 at 30 mg/kg once daily provided equivalent efficacy to that reported for BAY1895344 at 50 mg/kg twice daily when both were administered on a 3 days on/4 days off schedule (10).

Insights derived from preclinical studies facilitate optimization of the RP-3500 therapeutic index as a single agent and in combination with PARPi; firstly, by enrolling patients whose tumors have genetic vulnerabilities to ATR inhibition. For example, the *ATM*-deficient

RPE-1 cells were six-fold more sensitive to RP-3500 than *WT* RPE-1 cells. Further, *ATM*-deficient cells sustained irreversible RP-3500–mediated DNA damage over a 3-day exposure, unlike their *WT* counterparts. This is consistent with the results of Lloyd and colleagues (23), where AZD6738-induced DNA damage in the form of micronuclei was observed more quickly and at lower doses in FaDu *ATM* KO cells compared with FaDu *ATM* WT cells. Additional genetic vulnerabilities to ATRi have been identified through functional genomic screens (17–20) some of which now serve as clinical patient selection biomarkers. Furthermore, genetic profiles of innate replication stress have been identified in patients responsive to ATRi (43) or ATRi + topotecan (21) indicating a wide potential patient population for this drug class.

Secondly, the therapeutic index can be optimized with dose scheduling. The RP-3500 PK/efficacy relationship defined here illustrates that efficacy is influenced by the duration of daily target engagement and the duration of each treatment cycle. Our preclinical *in vitro* and *in vivo* studies suggest that, when using a continuous dosing schedule, 10 to 12 hours of 80% target engagement daily is required for minimum efficacy, whereas a 3- to 5-day treatment weekly is sufficient to maximize tumor cell killing if 80% target engagement is maintained during the treatment period. The increase in γH2AX that is proportional to efficacy suggests this to be a feasible molecular PD marker. The ability to maximize efficacy with a short duration of treatment allows flexibility for dosing holidays and increases tolerability by allowing recovery of bone marrow cells, given the reversible erythroid toxicity. Continuous daily administration of RP-3500 is limited by a reduction in RBC count and reticulocyte regeneration, consistent with the clinical findings of anemia with other ATRi (8, 14, 38, 44). Intermittent treatment is better tolerated with less anemia on a 3 days on/4 days off compared with 5 days on/2 days off or continuous daily administration schedules.

Optimizing the dosing schedule is particularly important in the context of ATRi/PARPi combinations, where overlapping clinical toxicities of single agent PARPi and ATRi include anemia, neutropenia, and thrombocytopenia (8, 14, 30). We demonstrate that continuous daily coadministration of RP-3500 and niraparib for several weeks in animal models is not tolerated, even at doses well below single-agent MTDs, consistent with previous preclinical (23, 24, 45) and clinical combination trials (44) with other ATRi. The concept of intermittent dosing of PARPi and ATRi was reported by Fang and colleagues and demonstrated good tolerability and efficacy with sequential PARPi followed by ATRi administration *in vivo*, compared with continuous administration of both agents together (24). However, this work did not provide a comparison of the proposed sequential schedule with concomitant intermittent scheduling. In contrast, our *in vitro* and *in vivo* results consistently demonstrate superior efficacy for concomitant versus sequential administration of PARPi followed by RP-3500. Supporting our observations in ATM-deficient tumor models, Lloyd and colleagues demonstrated sustained efficacy and less impact on body weight with full-dose olaparib in combination with half-dose AZD6738 with 3 days on/4 days off versus 5 days on/9 days off concomitant intermittent schedules (23). Our results demonstrate that, for RP-3500/PARPi combinations, introducing a weekly 4-day dose holiday allows for a resurgence of reticulocytes to regenerate the erythroid compartment; and that doses below the MTDs of each as single agents are sufficient for maximal efficacy. The increased tolerability and efficacy with this schedule are likely the result of two factors: (i) selective, irreparable DNA damage to DDR-defective tumor cells, and (ii) intermittent dose holidays allow for hematopoietic precursor cell maturation, minimizing anemia. Erythroid cell maturation, from early progenitor cells to mature enucleated reticulocytes, requires 2 to 7 days in mice and 7 to 9 days in humans (46, 47). A better understanding of the impact of RP-3500 on hematopoietic precursor cell injury and regeneration time following a dose holiday will dictate the intermittent scheduling of RP-3500 monotherapy or in combination with PARPi in clinic. The shorter half-lives of olaparib (12–18 hours; ref. 48) and niraparib (48–50 hours; ref. 49) among the PARPi are particularly amenable to intermittent clinical administration while talazoparib, with a half-life of 50 to 90 hours (50), is better suited to continuous administration. These results extend to the scheduling of ATRi combinations with other replication stress-inducing chemotherapeutic agents such as gemcitabine, platins, and topoisomerase inhibitors (14, 21, 51). Similar to PARPi, these agents are myelosuppressive and investigations incorporating intermittent ATRi administration warrant further investigation.

In summary, the results presented here demonstrate that RP-3500 is a potent ATRi with excellent selectivity over mTOR and other kinases. RP-3500 is highly efficacious in several ATM and BRCA1 LOF mouse models, with potential for tumor regression as a monotherapy. In xenograft models, intermittent administration 3 days on/4 days off weekly maximized efficacy while minimizing anemia. RP-3500 is highly effective in combination with PARPi when administered concomitantly on a short-term intermittent schedule rather than on continuous or sequential administration schedules. Preclinically, low-dose PARPi can be combined with RP-3500 to achieve dramatic and sustained antitumor responses on a schedule tolerated over several weeks. These results support the investigation of RP-3500 in an advanced phase I clinical study (NCT04497116) examining the short-term intermittent administration of RP-3500 as a monotherapy and in combination with low-dose PARPi as a potential means of achieving efficacy while alleviating anemia in clinical settings.

Authors' Disclosures

Authors' Contributions

A. Roulston: Conceptualization, formal analysis, supervision, writing–original draft, writing–review and editing. **M. Zimmermann:** Conceptualization, data curation, formal analysis, supervision, writing–review and editing. **R. Papp:** Conceptualization, data curation, formal analysis, supervision, writing–review and editing. **A. Skeldon:** Conceptualization, data curation, formal analysis. **C. Pellerin:** Conceptualization, data curation, formal analysis. **É. Dumas-Bérube:** Data curation, formal analysis. **V. Dumais:** Data curation, formal analysis. **S. Dorich:** Conceptualization, data curation, formal analysis. **L.D. Fader:** Conceptualization, supervision. **S. Fournier:** Data curation, formal analysis. **L. Li:** Data curation, formal analysis. **M.-E. Leclaire:** Data curation, formal analysis. **S.Y. Yin:** Data curation, formal analysis. **A. Chefson:** Data curation, formal analysis. **H. Alam:** Data curation, formal analysis. **W. Yang:** Data curation, formal analysis. **C. Fugère-Desjardins:** Data curation, formal analysis. **S. Vignini-Hammond:** Data curation, formal analysis. **K. Skorey:** Conceptualization, data curation, formal analysis. **A. Mulani:** Data curation, formal analysis. **V. Rimkunas:** Conceptualization, data curation, formal analysis. **A. Veloso:** Data curation, formal analysis. **M. Hamel:** Conceptualization. **R. Stocco:** Conceptualization. **Y. Mamane:** Conceptualization, supervision. **Z. Li:** Formal analysis, supervision. **J. Young:** Supervision. **M. Zinda:** Conceptualization, supervision, writing–review and editing. **W.C. Black:** Conceptualization, supervision, writing–review and editing.

Acknowledgments

References

1. Pilie PG, Tang C, Mills GB, Yap TA. State-of-the-art strategies for targeting the DNA damage response in cancer. Nat Rev Clin Oncol 2019;16:81–104.
2. Blackford AN, Jackson SP. ATM, ATR, and DNA-PK: The trinity at the heart of the DNA damage response. Mol Cell 2017;66:801–17.
3. Lecona E, Fernandez-Capetillo O. Targeting ATR in cancer. Nat Rev Cancer 2018;18:586–95.
4. Toledo LI, Altmeyer M, Rask MB, Lukas C, Larsen DH, Povlsen LK, et al. ATR prohibits replication catastrophe by preventing global exhaustion of RPA. Cell 2013;155:1088–103.
5. Foote KM, Nissink JWM, McGuire T, Turner P, Guichard S, Yates JWT, et al. Discovery and characterization of AZD6738, a potent inhibitor of ataxia telangiectasia mutated and Rad3 related (ATR) kinase with application as an anticancer agent. J Med Chem 2018;61:9889–907.
6. Saldivar JC, Hamperl S, Bocek MJ, Chung M, Bass TE, Cisneros-Soberanis F, et al. An intrinsic S/G2 checkpoint enforced by ATR. Science 2018;361: 806–10.
7. Dillon MT, Boylan Z, Smith D, Guevara J, Mohammed K, Peckitt C, et al. PATRIOT: A phase I study to assess the tolerability, safety and biological effects of a specific ataxia telangiectasia and Rad3-related (ATR) inhibitor (AZD6738) as a single agent and in combination with palliative radiation therapy in patients with solid tumours. Clin Transl Radiat Oncol 2018;12: 16–20.
8. Dillon M, Guevara J, Mohammed K, Smith SA, Dean E, McLellan L, et al. A phase I study of ATR inhibitor, AZD6738, as monotherapy in advanced solid tumours (PATRIOT part A, B). Ann Oncol 2019;30:v165–v6.
9. Jo U, Senatorov IS, Zimmermann A, Saha LK, Murai Y, Kim SH, et al. Novel and highly potent ATR inhibitor M4344 kills cancer cells with replication stress, and enhances the chemotherapeutic activity of widely used DNA damaging agents. Mol Cancer Ther 2021;20:1431–41.
10. Wengner AM, Siemeister G, Lucking U, Lefranc J, Wortmann L, Lienau P, et al. The novel ATR inhibitor BAY 1895344 is efficacious as monotherapy and combined with DNA damage-inducing or repair-compromising therapies in preclinical cancer models. Mol Cancer Ther 2020;19:26–38.
11. Yap TA, Tan DSP, Terbuch A, Caldwell R, Guo C, Goh BC, et al. First-in-human trial of the oral ataxia telangiectasia and RAD3-related (ATR) inhibitor BAY 1895344 in patients with advanced solid tumors. Cancer Discov 2021;11:80–91.
12. Yap TA, Tolcher AW, Plummer E, Becker A, Fleuranceau-Morel P, Goddemeier T, et al. A first-in-human phase I study of ATR inhibitor M1774 in patients with solid tumors. J Clin Oncol 2021;39:TPS3153–TPS.
13. Mei L, Zhang J, He K, Zhang J. Ataxia telangiectasia and Rad3-related inhibitors and cancer therapy: where we stand. J Hematol Oncol 2019;12:43.
14. Yap TA, O'Carrigan B, Penney MS, Lim JS, Brown JS, de Miguel Luken MJ, et al. Phase I trial of first-in-class ATR inhibitor M6620 (VX-970) as monotherapy or in combination with carboplatin in patients with advanced solid tumors. J Clin Oncol 2020;38:3195–204.
15. Eder JP, Sohal D, Mahdi H, Do K, Keedy V, Hafez N, et al. Abstract A080: Olaparib and the ATR inhibitor AZD6738 in relapsed, refractory cancer patients with homologous recombination (HR) repair mutations–OLAPCO. Mol Cancer Ther 2019;18:A080–A.
16. Middleton FK, Patterson MJ, Elstob CJ, Fordham S, Herriott A, Wade MA, et al. Common cancer-associated imbalances in the DNA damage response confer sensitivity to single agent ATR inhibition. Oncotarget 2015;6:32396–409.
17. Reaper PM, Griffiths MR, Long JM, Charrier JD, Maccormick S, Charlton PA, et al. Selective killing of ATM- or p53-deficient cancer cells through inhibition of ATR. Nat Chem Biol 2011;7:428–30.
18. Hustedt N, Alvarez-Quilon A, McEwan A, Yuan JY, Cho T, Koob L, et al. A consensus set of genetic vulnerabilities to ATR inhibition. Open Biol 2019;9: 190156.
19. Menezes DL, Holt J, Tang Y, Feng J, Barsanti P, Pan Y, et al. A synthetic lethal screen reveals enhanced sensitivity to ATR inhibitor treatment in mantle cell lymphoma with ATM loss-of-function. Mol Cancer Res 2015;13:120–9.
20. Wang C, Wang G, Feng X, Shepherd P, Zhang J, Tang M, et al. Genome-wide CRISPR screens reveal synthetic lethality of RNASEH2 deficiency and ATR inhibition. Oncogene 2019;38:2451–63.
21. Thomas A, Takahashi N, Rajapakse VN, Zhang X, Sun Y, Ceribelli M, et al. Therapeutic targeting of ATR yields durable regressions in small cell lung cancers with high replication stress. Cancer Cell 2021;39:566–79.
22. Kim H, George E, Ragland R, Rafail S, Zhang R, Krepler C, et al. Targeting the ATR/CHK1 axis with PARP inhibition results in tumor regression in BRCA-mutant ovarian cancer models. Clin Cancer Res 2017;23:3097–108.
23. Lloyd RL, Wijnhoven PWG, Ramos-Montoya A, Wilson Z, Illuzzi G, Falenta K, et al. Combined PARP and ATR inhibition potentiates genome instability and cell death in ATM-deficient cancer cells. Oncogene 2020;39:4869–83.
24. Fang Y, McGrail DJ, Sun C, Labrie M, Chen X, Zhang D, et al. Sequential therapy with PARP and WEE1 inhibitors minimizes toxicity while maintaining efficacy. Cancer Cell 2019;35:851–67.
25. Yazinski SA, Comaills V, Buisson R, Genois MM, Nguyen HD, Ho CK, et al. ATR inhibition disrupts rewired homologous recombination and fork protection pathways in PARP inhibitor-resistant BRCA-deficient cancer cells. Genes Dev 2017;31:318–32.
26. Schoonen PM, Kok YP, Wierenga E, Bakker B, Foijer F, Spierings DCJ, et al. Premature mitotic entry induced by ATR inhibition potentiates olaparib inhibition-mediated genomic instability, inflammatory signaling, and cytotoxicity in BRCA2-deficient cancer cells. Mol Oncol 2019;13:2422–40.
27. Krebs MG, Lopez J, El-Khoueiry A, Bang Y-J, Postel-Vinay S, Abida W, et al. Abstract CT026: Phase I study of AZD6738, an inhibitor of ataxia telangiectasia Rad3-related (ATR), in combination with olaparib or durvalumab in patients (pts) with advanced solid cancers. Cancer Res 2018;78:CT026–CT.
28. Murai J, Pommier Y. PARP trapping beyond homologous recombination and platinum sensitivity in cancers. Annual Review of Cancer Biology 2019;3:131–50.

29. Jette NR, Radhamani S, Arthur G, Ye R, Goutam S, Bolyos A, et al. Combined poly-ADP ribose polymerase and ataxia-telangiectasia mutated/Rad3-related inhibition targets ataxia-telangiectasia mutated-deficient lung cancer cells. Br J Cancer 2019;121:600–10.

30. Pilie PG, Gay CM, Byers LA, O'Connor MJ, Yap TA. PARP inhibitors: Extending benefit beyond BRCA-mutant cancers. Clin Cancer Res 2019;25: 3759–71.

31. Crane SN, Truong VL, Abdoli A, Truchon J-F, Black C, Dorich S, et al. Inventors; Repare Therapeutics Inc., assignee. Compounds, pharmaceutical compositions, and methods of preparing compounds and of their use as ATR kinase inhibitors Patent WO/2020087170 pending. 2020, May 7.

32. Ianevski A, He L, Aittokallio T, Tang J. SynergyFinder: a web application for analyzing drug combination dose-response matrix data. Bioinformatics 2020;36: 2645.

33. Patricelli MP, Nomanbhoy TK, Wu J, Brown H, Zhou D, Zhang J, et al. In situ kinase profiling reveals functionally relevant properties of native kinases. Chem Biol 2011;18:699–710.

34. Buisson R, Boisvert JL, Benes CH, Zou L. Distinct but concerted roles of ATR, DNA-PK, and Chk1 in countering replication stress during S phase. Mol Cell 2015;59:1011–24.

35. Giannini G, Ristori E, Cerignoli F, Rinaldi C, Zani M, Viel A, et al. Human MRE11 is inactivated in mismatch repair-deficient cancers. EMBO Rep 2002;3: 248–54.

36. Ghandi M, Huang FW, Jane-Valbuena J, Kryukov GV, Lo CC, McDonald ER 3rd, et al. Next-generation characterization of the Cancer Cell Line Encyclopedia. Nature 2019;569:503–8.

37. Chen T, Middleton FK, Falcon S, Reaper PM, Pollard JR, Curtin NJ. Development of pharmacodynamic biomarkers for ATR inhibitors. Mol Oncol 2015;9: 463–72.

38. Thomas A, Redon CE, Sciuto L, Padiernos E, Ji J, Lee MJ, et al. Phase I study of ATR inhibitor M6620 in combination with topotecan in patients with advanced solid tumors. J Clin Oncol 2018;36:1594–602.

39. Elstrodt F, Hollestelle A, Nagel JH, Gorin M, Wasielewski M, van den Ouweland A, et al. BRCA1 mutation analysis of 41 human breast cancer cell lines reveals three new deleterious mutants. Cancer Res 2006;66:41–5.

40. Zenke FT, Zimmermann A, Dahmen H, Elenbaas B, Pollard J, Reaper P, et al. Abstract 369: Antitumor activity of M4344, a potent and selective ATR inhibitor, in monotherapy and combination therapy [abstract]. In: Proceedings of the American Association for Cancer Research Annual Meeting 2019; 2019 Mar 29– Apr 3; Atlanta, GA. Philadelphia (PA): AACR; Cancer Res 2019;79 (13 Suppl): Abstract nr 369.

41. Vendetti FP, Karukonda P, Clump DA, Teo T, Lalonde R, Nugent K, et al. ATR kinase inhibitor AZD6738 potentiates CD8+ T cell-dependent antitumor activity following radiation. J Clin Invest 2018;128:3926–40.

42. Vendetti FP, Lau A, Schamus S, Conrads TP, O'Connor MJ, Bakkenist CJ. The orally active and bioavailable ATR kinase inhibitor AZD6738 potentiates the anti-tumor effects of cisplatin to resolve ATM-deficient non-small cell lung cancer in vivo. Oncotarget 2015;6:44289–305.

43. Dreyer SB, Upstill-Goddard R, Paulus-Hock V, Paris C, Lampraki EM, Dray E, et al. Targeting DNA damage response and replication stress in pancreatic cancer. Gastroenterology 2021;160:362–77.

44. Berges A, Cheung A, Pierce A, Dean E, Felicetti B, Standifer N, et al. Abstract CT118: PK-biomarker-safety modelling aids choice of recommended phase II dose and schedule for AZD6738 (ATR inhibitor). Cancer Res 2018;78: CT118–CT.

45. Kim H, Xu H, George E, Hallberg D, Kumar S, Jagannathan V, et al. Combining PARP with ATR inhibition overcomes PARP inhibitor and platinum resistance in ovarian cancer models. Nat Commun 2020;11:3726.

46. Palis J. Primitive and definitive erythropoiesis in mammals. Front Physiol 2014;5:3.

47. Hattangadi SM, Wong P, Zhang L, Flygare J, Lodish HF. From stem cell to red cell: regulation of erythropoiesis at multiple levels by multiple proteins, RNAs, and chromatin modifications. Blood 2011;118:6258–68.

48. Rolfo C, Swaisland H, Leunen K, Rutten A, Soetekouw P, Slater S, et al. Effect of food on the pharmacokinetics of olaparib after oral dosing of the capsule formulation in patients with advanced solid tumors. Adv Ther 2015;32:510–22.

49. Moore K, Zhang ZY, Agarwal S, Burris H, Patel MR, Kansra V. The effect of food on the pharmacokinetics of niraparib, a poly(ADP-ribose) polymerase (PARP) inhibitor, in patients with recurrent ovarian cancer. Cancer Chemother Pharmacol 2018;81:497–503.

50. Yu Y, Chung CH, Plotka A, Quinn K, Shi H, Papai Z, et al. A phase 1 mass balance study of (14) c-labeled talazoparib in patients with advanced solid tumors. J Clin Pharmacol 2019;59:1195–203.

51. Konstantinopoulos PA, Cheng SC, Wahner Hendrickson AE, Penson RT, Schumer ST, Doyle LA, et al. Berzosertib plus gemcitabine versus gemcitabine alone in platinum-resistant high-grade serous ovarian cancer: a multicentre, open-label, randomised, phase 2 trial. Lancet Oncol 2020;21:957–68.